Electronic Supplementary Material (ESI) for Journal of Materials Chemistry A.
This journal is © The Royal Society of Chemistry 2017

Supporting Information

Ultrahigh rate sodium ion storage with nitrogen-doped expanded graphite oxide in ether-based electrolyte

Mingxiang Hu[a], Hongjiang Zhou[a], Xin Gan[a], Le Yang[a], Zheng-Hong Huang[a,b], Da-Wei Wang[c], Feiyu Kang[a,b], Ruitao Lv[a,b,*]

[a] *State Key Laboratory of New Ceramics and Fine Processing, School of Materials Science and Engineering, Tsinghua University, Beijing 100084, China*

[b] *Key Laboratory of Advanced Materials (MOE), School of Materials Science and Engineering, Tsinghua University, Beijing 100084, China*

[c] *School of Chemical Engineering, The University of New South Wales, Sydney, NSW 2052, Australia*

* Addresses correspondence to lvruitao@tsinghua.edu.cn

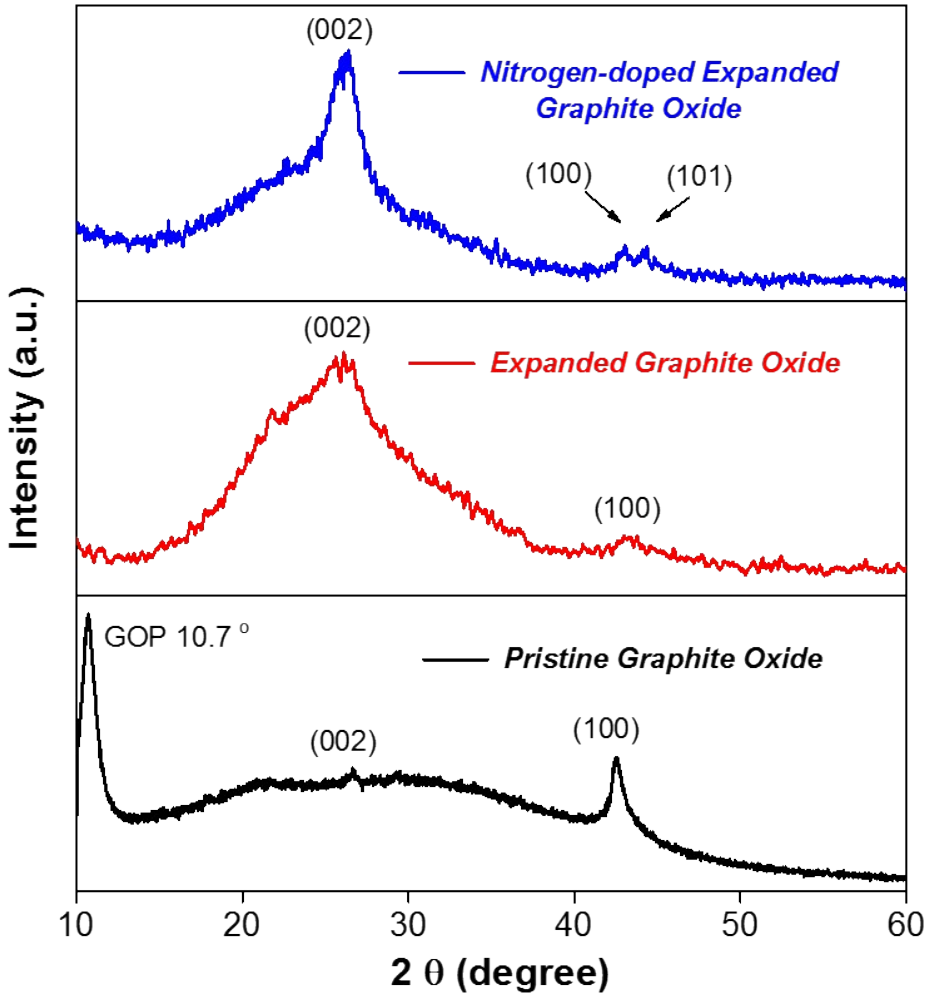

Figure S1. XRD patterns of nitrogen-doped expanded graphite oxide (NEGO), expanded graphite oxide (EGO) and pristine graphite oxide (GO).

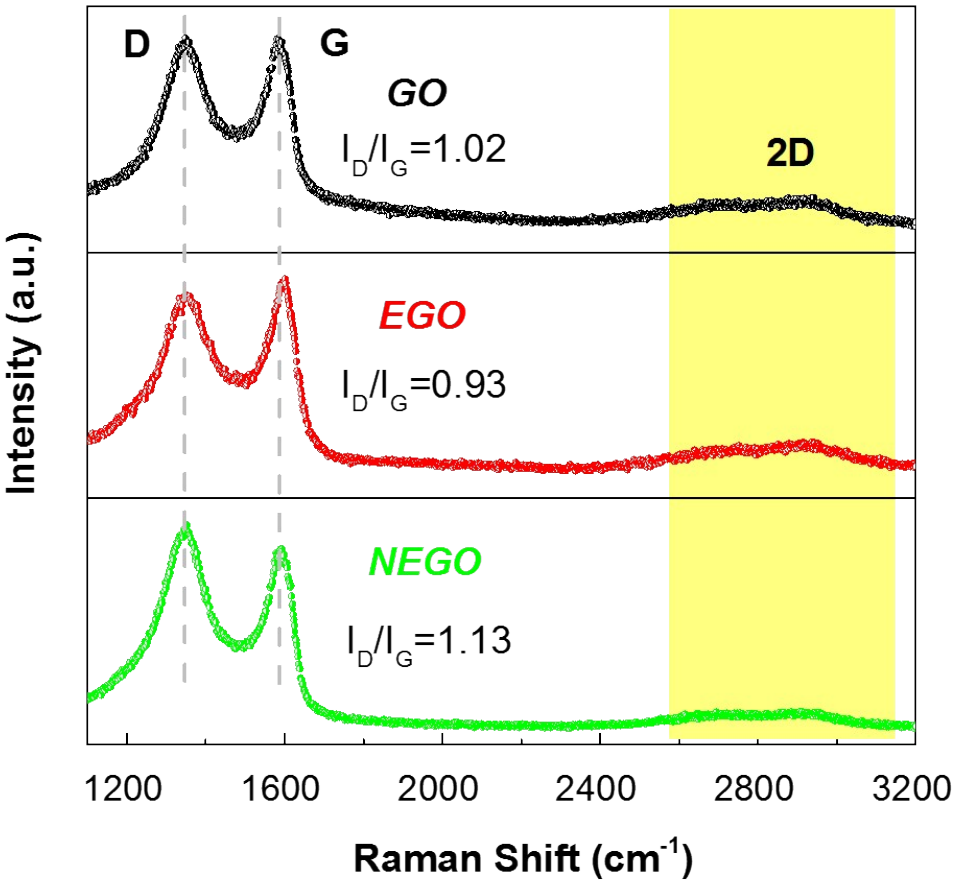

Figure S2. Raman spectra of different samples.

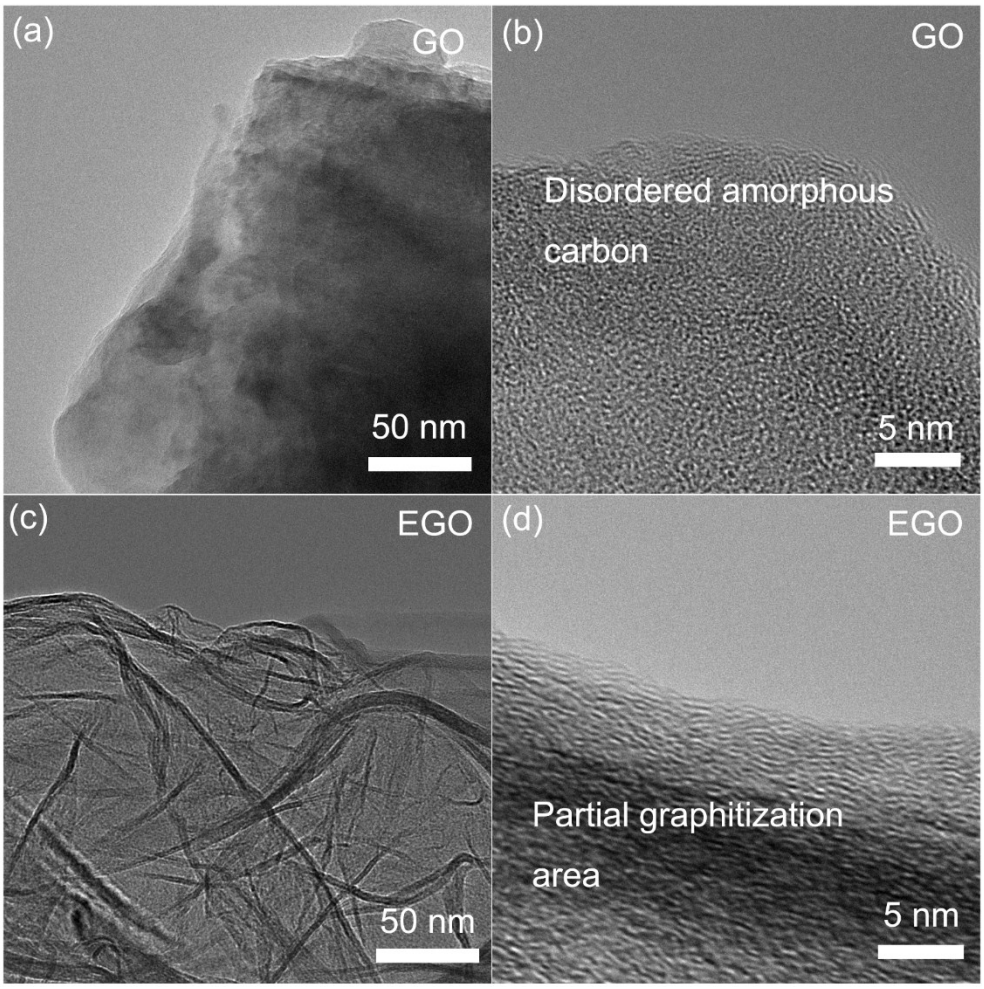

Figure S3. TEM images of (a) GO and (b) EGO; HRTEM images of (c) GO and (d) EGO.

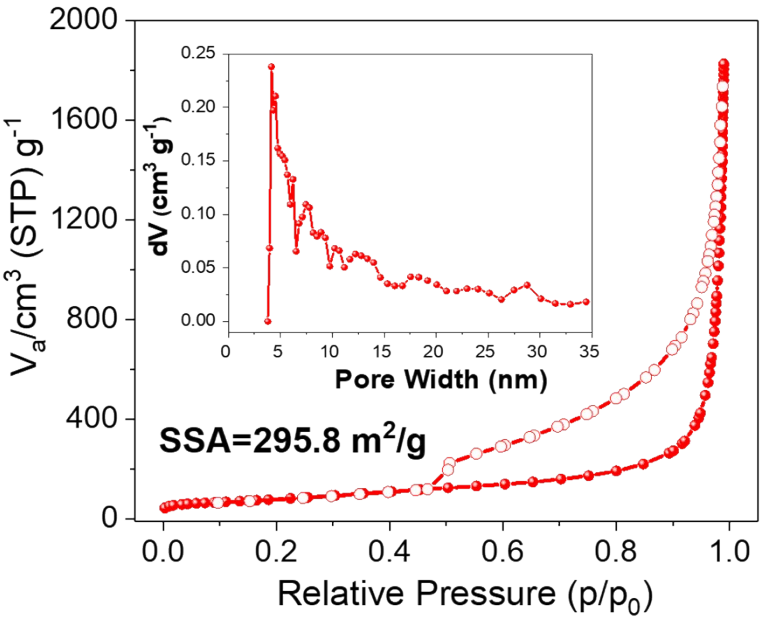

Figure S4. N_2 isotherm absorption-desorption curve of NEGO sample; Inset is the corresponding pore size distribution.

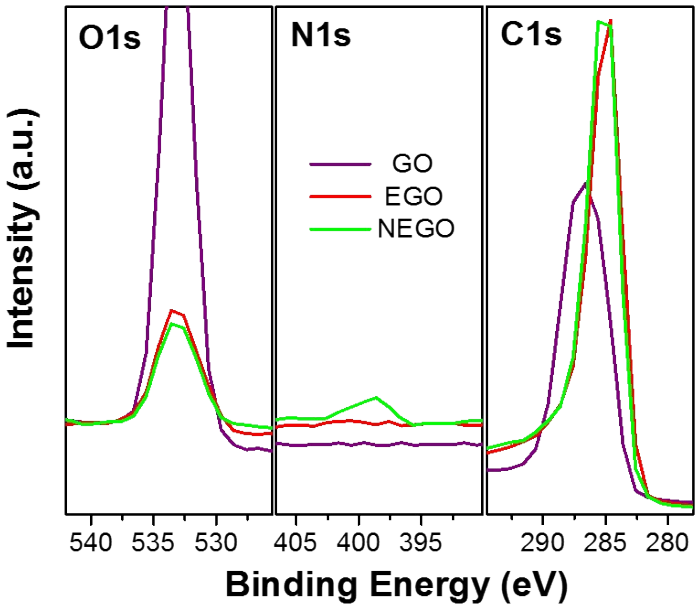

Figure S5. Comparison of the XPS survey spectra of GO, EGO and NEGO.

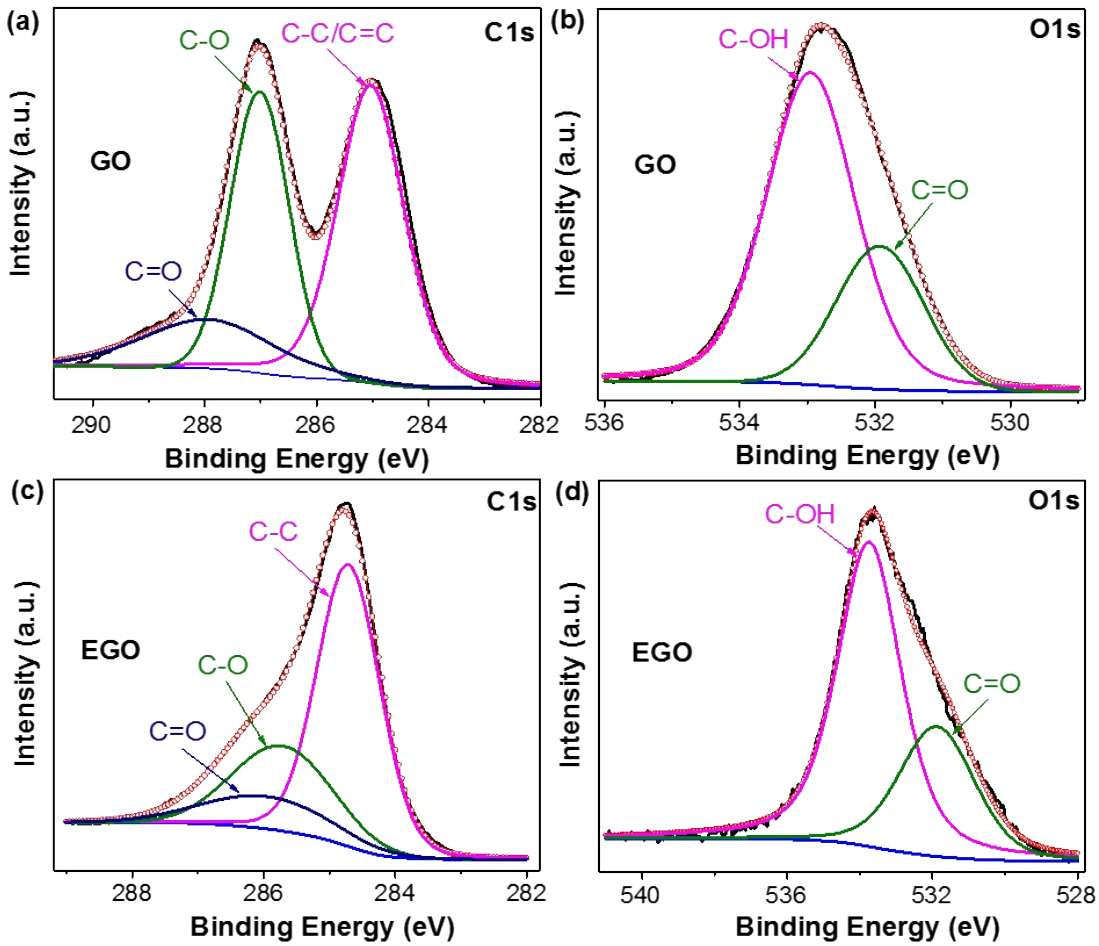

Figure S6. High-resolution XPS spectra of C 1s and N 1s: (a, b) GO; (c, d) EGO.

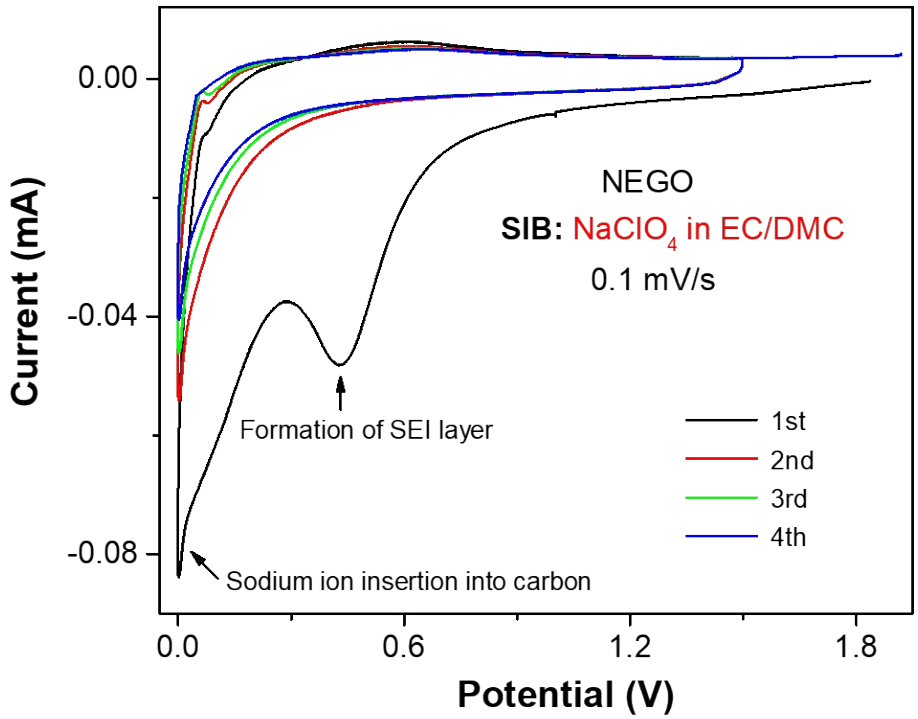

Figure S7. CV curves of NEGO in the voltage range of 0-1.0 V with a scan rate of 0.1 mV/s as anode material for SIBs (electrolyte: $NaClO_4$ in EC/DMC).

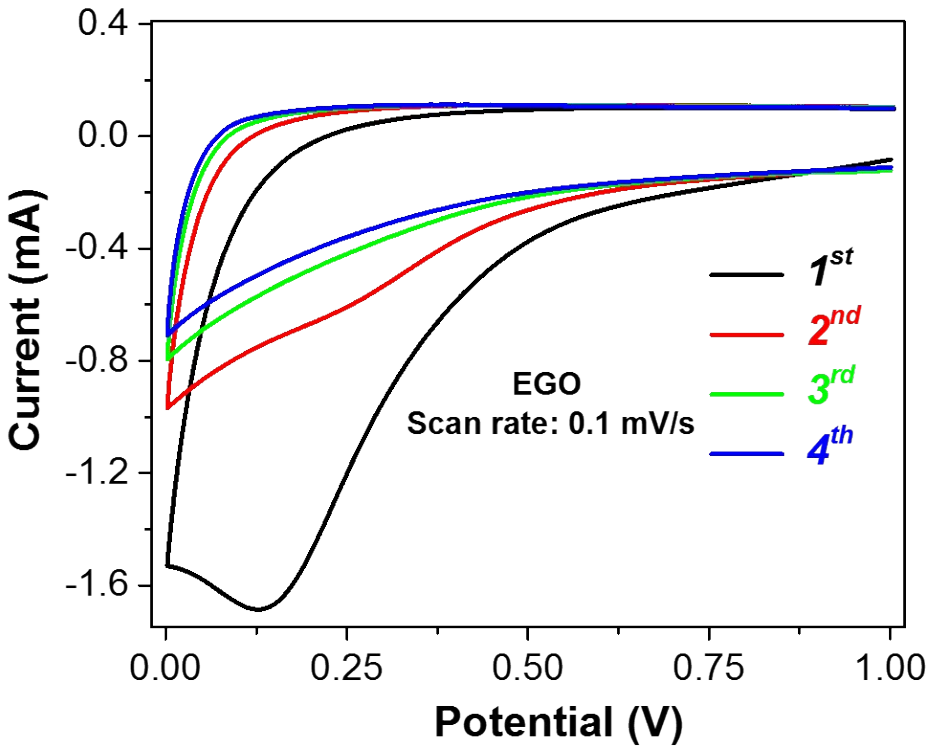

Figure S8. CV curves of EGO in the voltage range of 0-1.0 V with a scan rate of 0.1 mV/s as anode material for SIBs (electrolyte: $NaClO_4$ in EC/DMC).

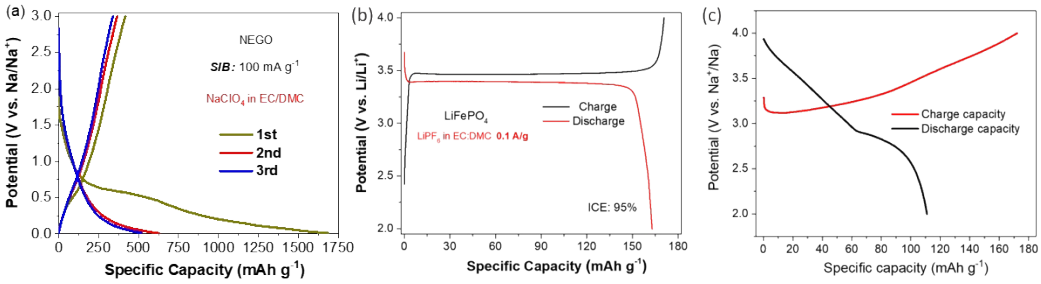

Figure S9. (a) Galvanostatic charge–discharge profiles of the first three cycles of NEGO in EC/DMC at a current density of 0.1 A g^{-1}. The Galvanostatic charge/discharge profiles of (b) $LiFePO_4$ in lithium ion battery at 0.1 A/g and (c) O3-$Na_{0.9}[Cu_{0.22}Fe_{0.30}Mn_{0.48}]O_2$ in sodium ion battery at 0.1 A/g.

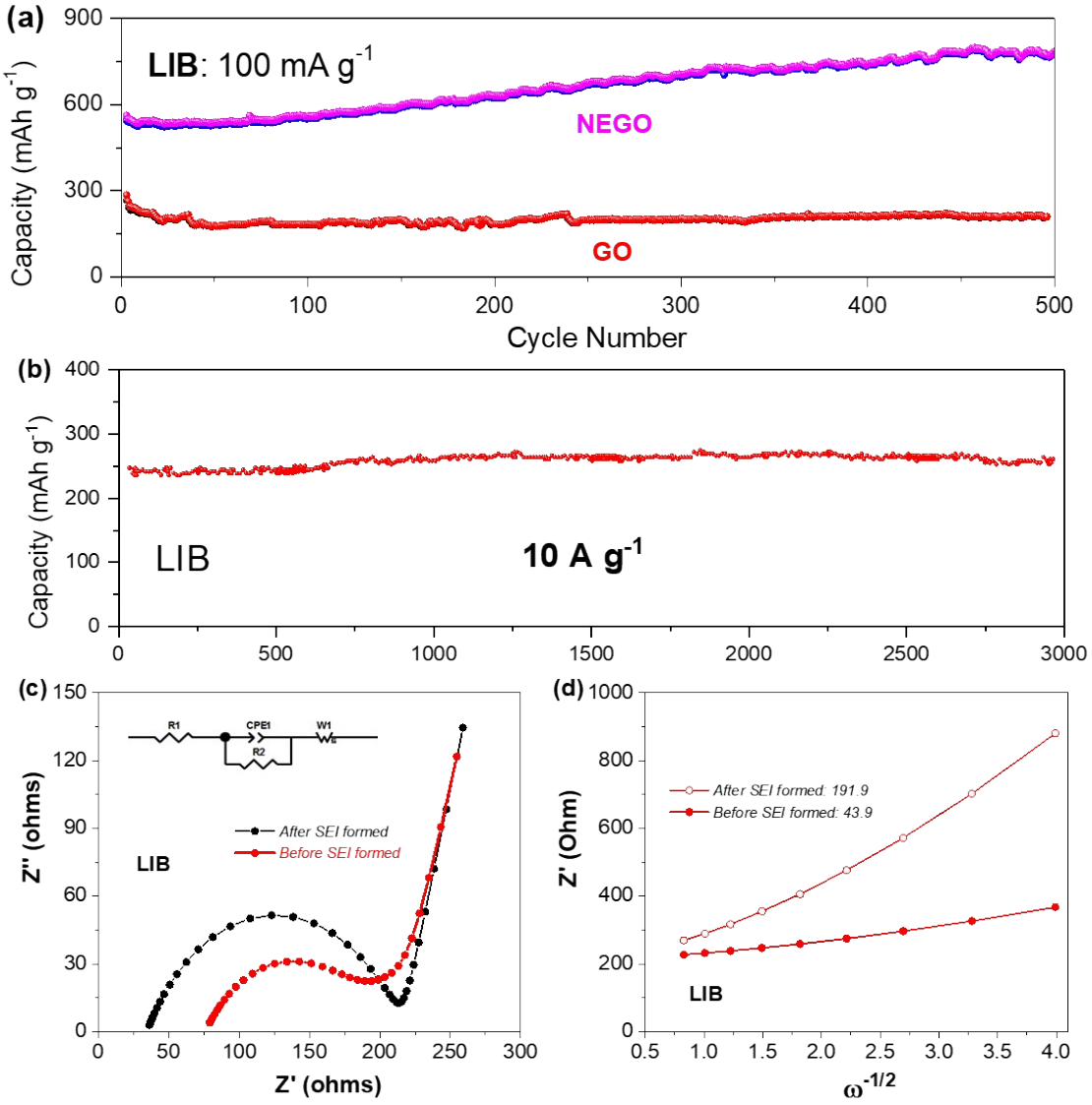

Figure S10. (a) Cycling performance of GO and NEGO in lithium-ion battery (LIB) under 100 mA g^{-1}; (b) long-term cycle performance of NEGO as anode of LIB under 10 A g^{-1}; (c) Electrochemical impedance spectra of NEGO before and after the formation of SEI in LIB. (d) Dependence of Z' on $\omega^{-1/2}$ of NEGO in LIB before and after the formation of SEI. Here Z' denotes the real part of impedance and ω denotes angular frequency. The straight lines are the corresponding linear fitting plots.

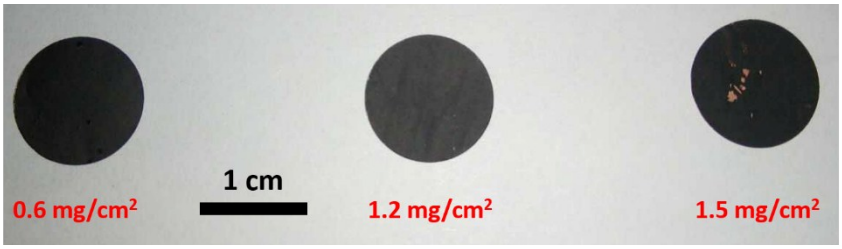

Figure S11. Comparison of NEGO coatings on copper foils with different loading masses.

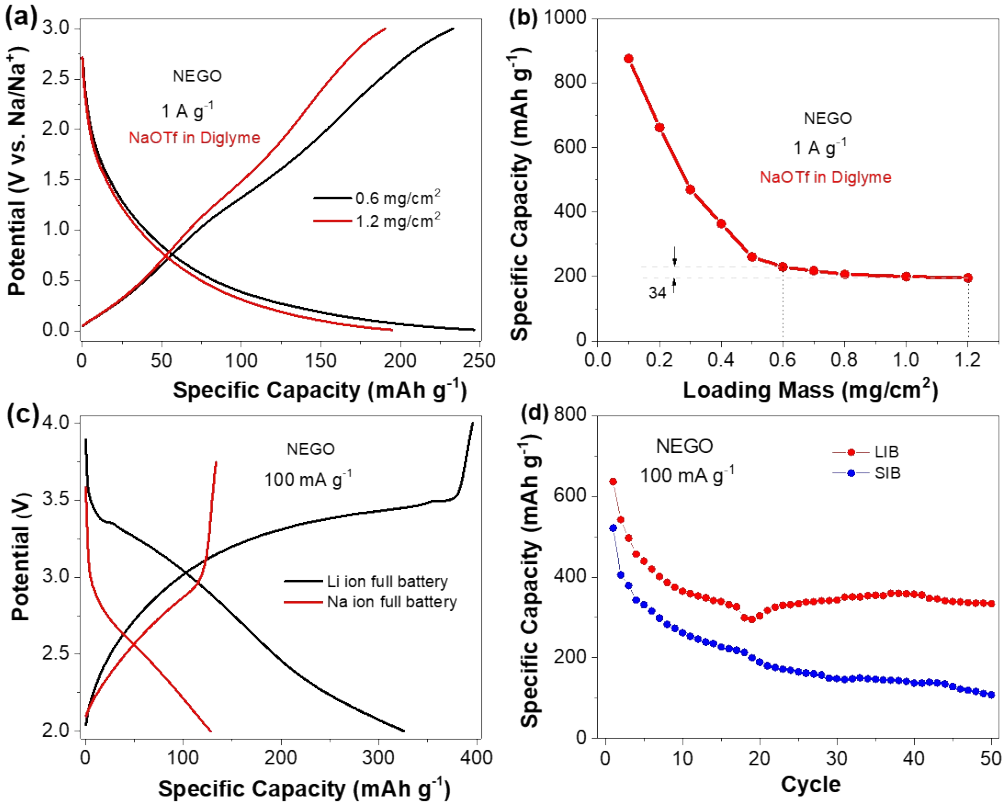

Figure S12. Comparison of the electrochemical performance of NEGO with different loading mass in ester-based solvents. (a) Galvanostatic charge–discharge profiles of NEGO for the loading mass of 0.6 and 1.2 mg/cm^2. (b) Dependence of the capacity on the loading mass of NEGO in the anode of SIBs (electrolyte: DIGLYME). (c) Galvanostatic charge–discharge profiles of NEGO as the anode in lithium-ion full battery and sodium-ion full battery under 100 mA g^{-1}. (d) Cycle performances of NEGO as the anode in lithium-ion full battery and sodium-ion full battery under 100 mA g^{-1}.

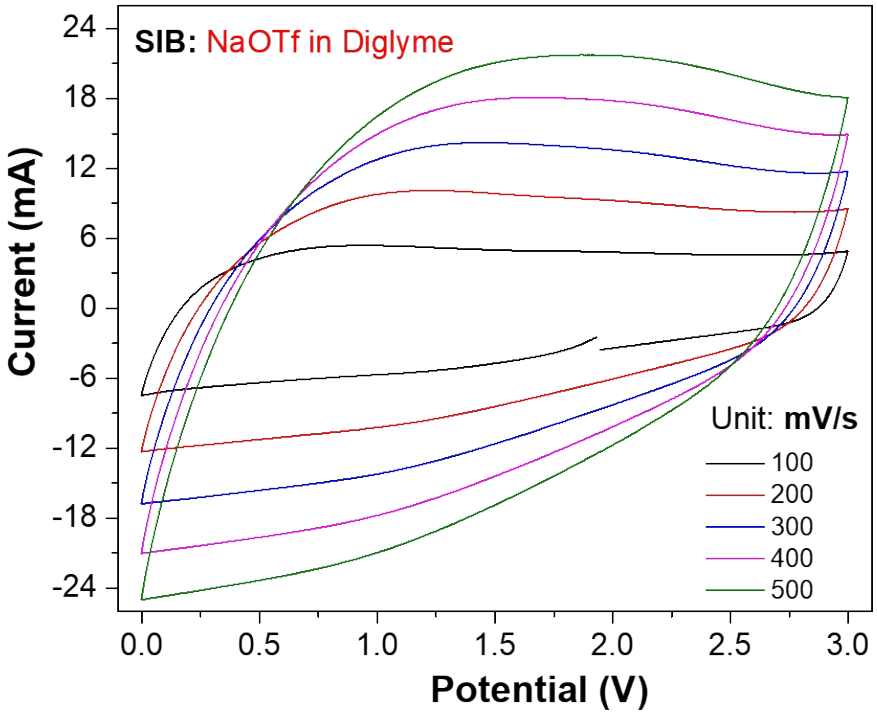

Figure S13. CV curves of NEGO at various scan rates from 100 mV s^{-1} to 500 mV s^{-1} as the anode material for SIBs (NaOTf in DIGLYME).

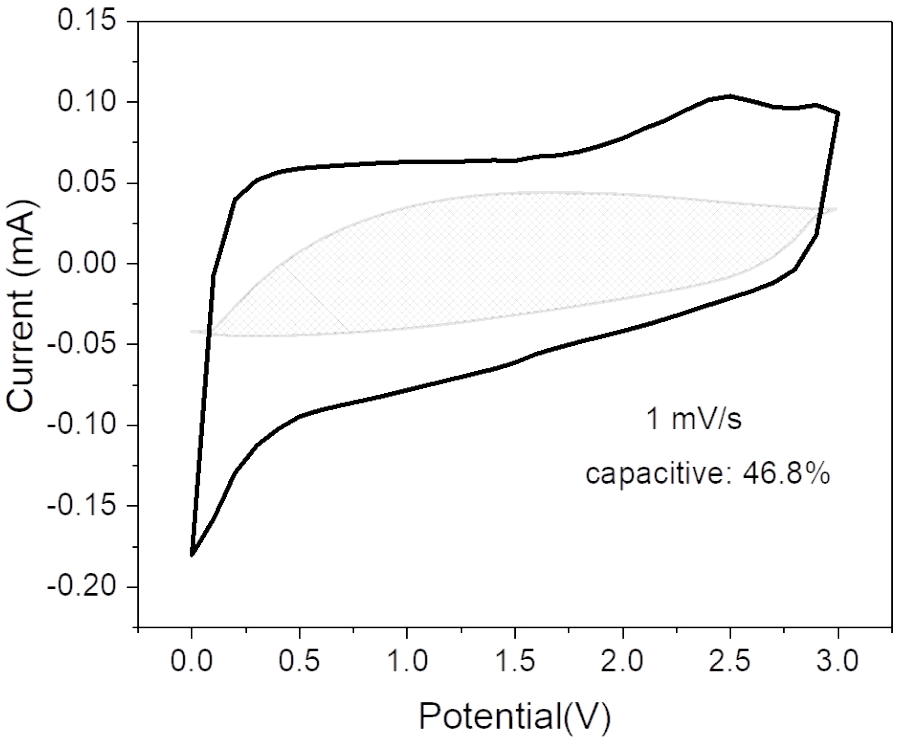

Figure S14. CV curves of NEGO as anode material for SIBs in DIGLYME with the capacitive contribution to the reduction process shown by the shaded region at 1 mV/s scan rate.

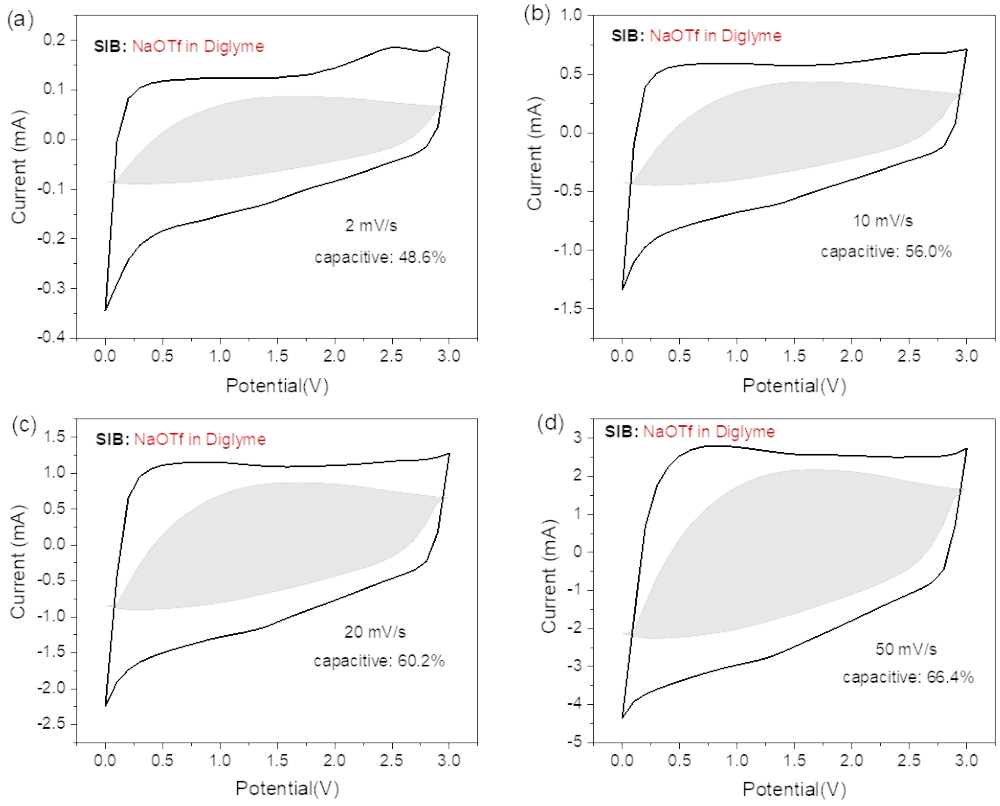

Figure S15. CV curves of NEGO as anode material for SIBs in DIGLYME with the capacitive contribution to the reduction process shown by the shaded region at (a) 2 mV/s; (b) 10 mV/s; (c) 20 mV/s and (d) 50 mV/s scan rate.

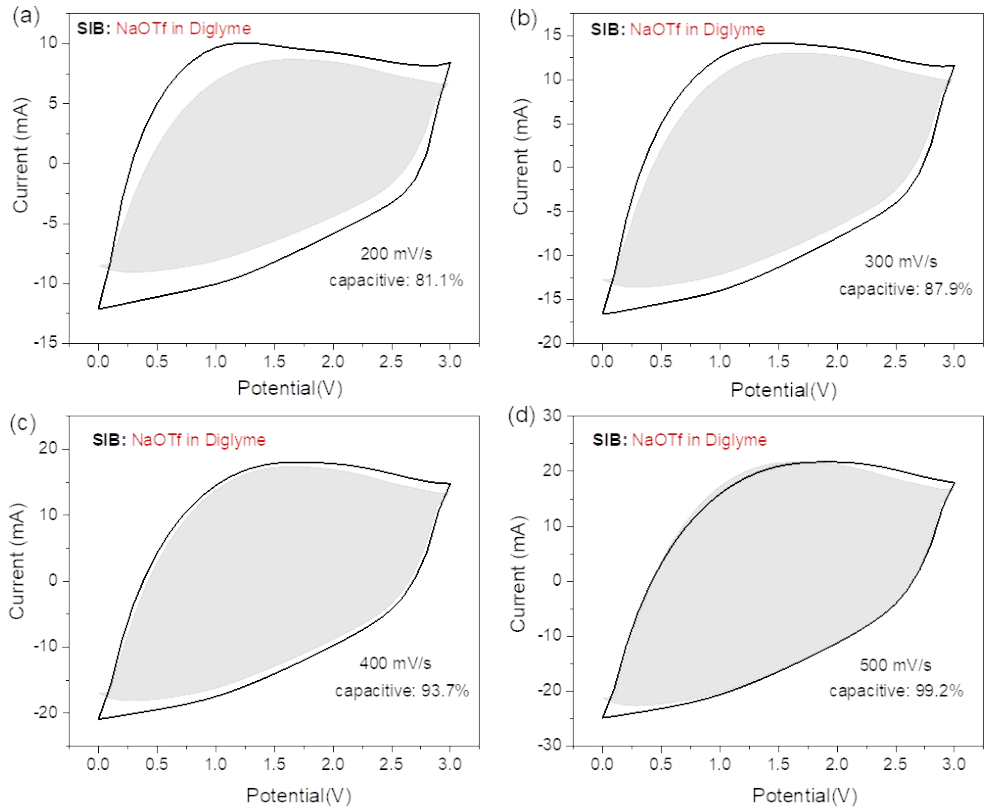

Figure S16. CV curves of NEGO as anode material for SIBs in DIGLYME with the capacitive contribution to the reduction process shown by the shaded region at (a) 200 mV/s; (b) 300 mV/s; (c) 400 mV/s and (d) 500 mV/s scan rate.

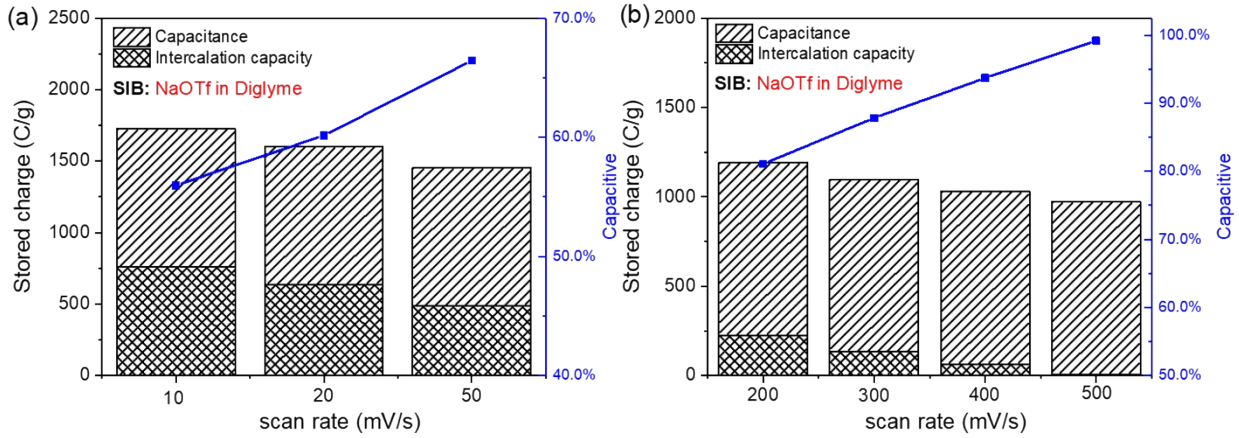

Figure S17. Contributions of capacitive capacitance with the scan rate of NEGO as the anode material for SIBs in DIGLYME electrolytes.

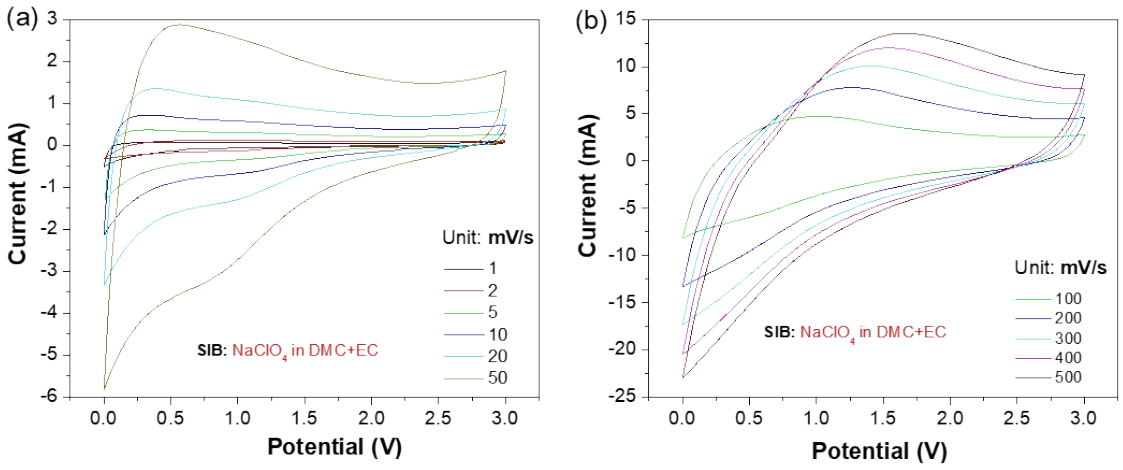

Figure S18. CV curves of NEGO as anode material for SIBs in ester-based electrode (EC/DMC) with the scan rate from 1 mV/s to 500 mV/s.

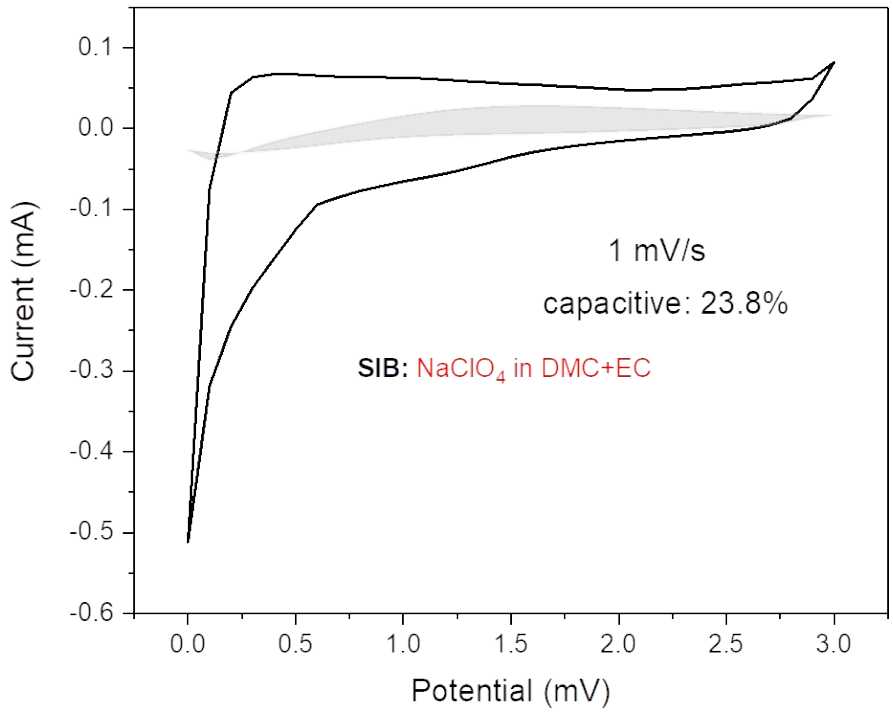

Figure S19. CV curves of NEGO as anode material for SIBs in EC/DMC with the capacitive contribution to the reduction process shown by the shaded region at the scan rate of 1 mV/s.

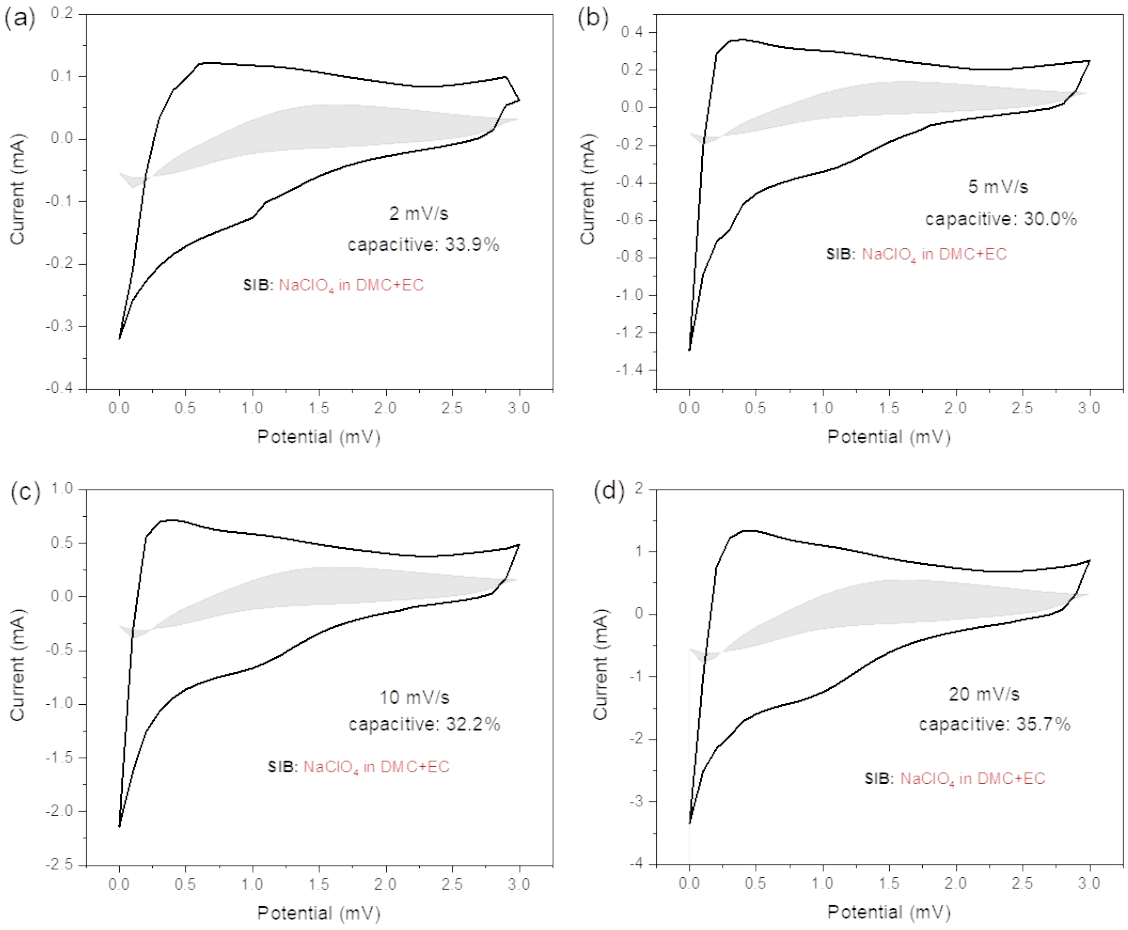

Figure S20. CV curves of NEGO as anode material for SIBs in EC/DMC with the capacitive contribution to the reduction process shown by the shaded region at the scan rates of (a) 2 mV/s; (b) 5 mV/s; (c) 10 mV/s and (d) 20 mV/s.

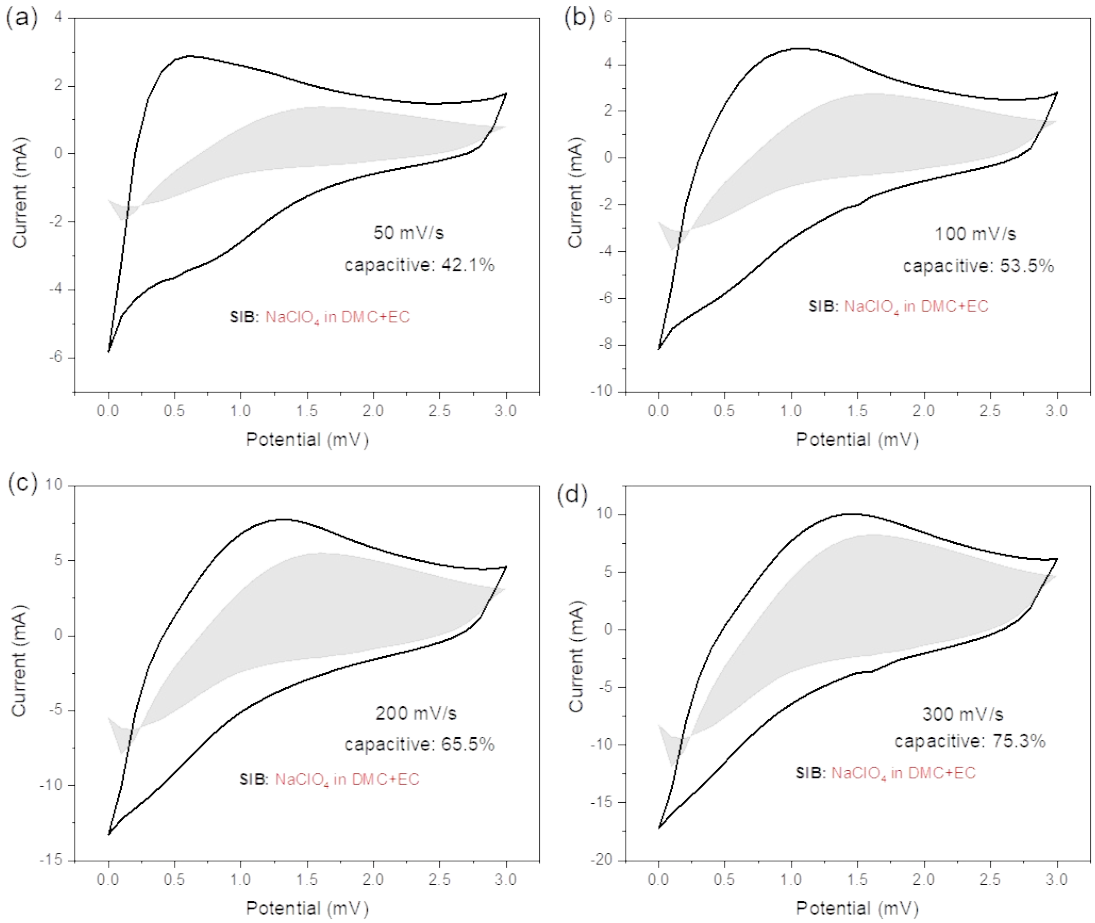

Figure S21. CV curves of NEGO as anode material for SIBs in EC/DMC with the capacitive contribution to the reduction process shown by the shaded region at the scan rate of (a) 50 mV/s; (b) 100 mV/s; (c) 200 mV/s and (d) 300 mV/s.

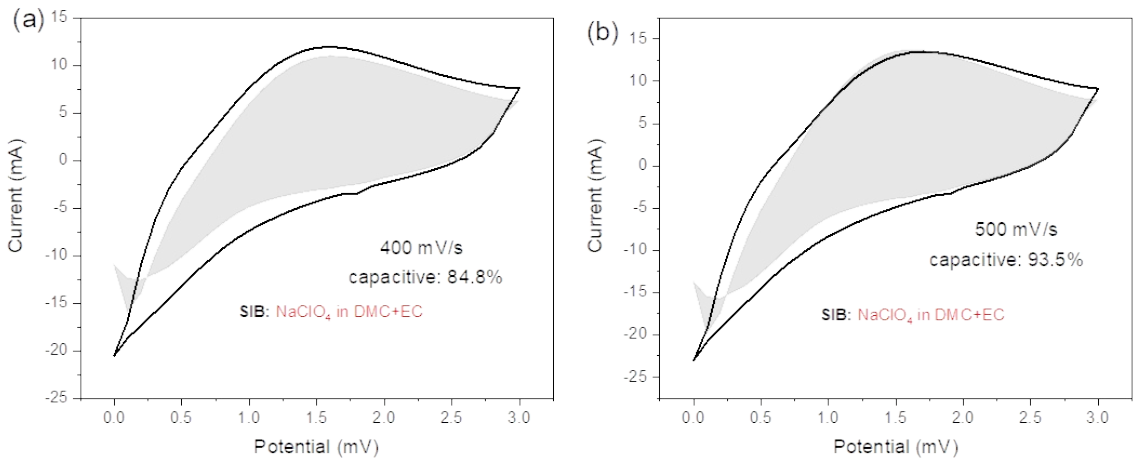

Figure S22. CV curves of NEGO as anode material for SIBs in EC/DMC with the capacitive contribution to the reduction process shown by the shaded region at the scan rate of (a) 400 mV/s and (b) 500 mV/s.

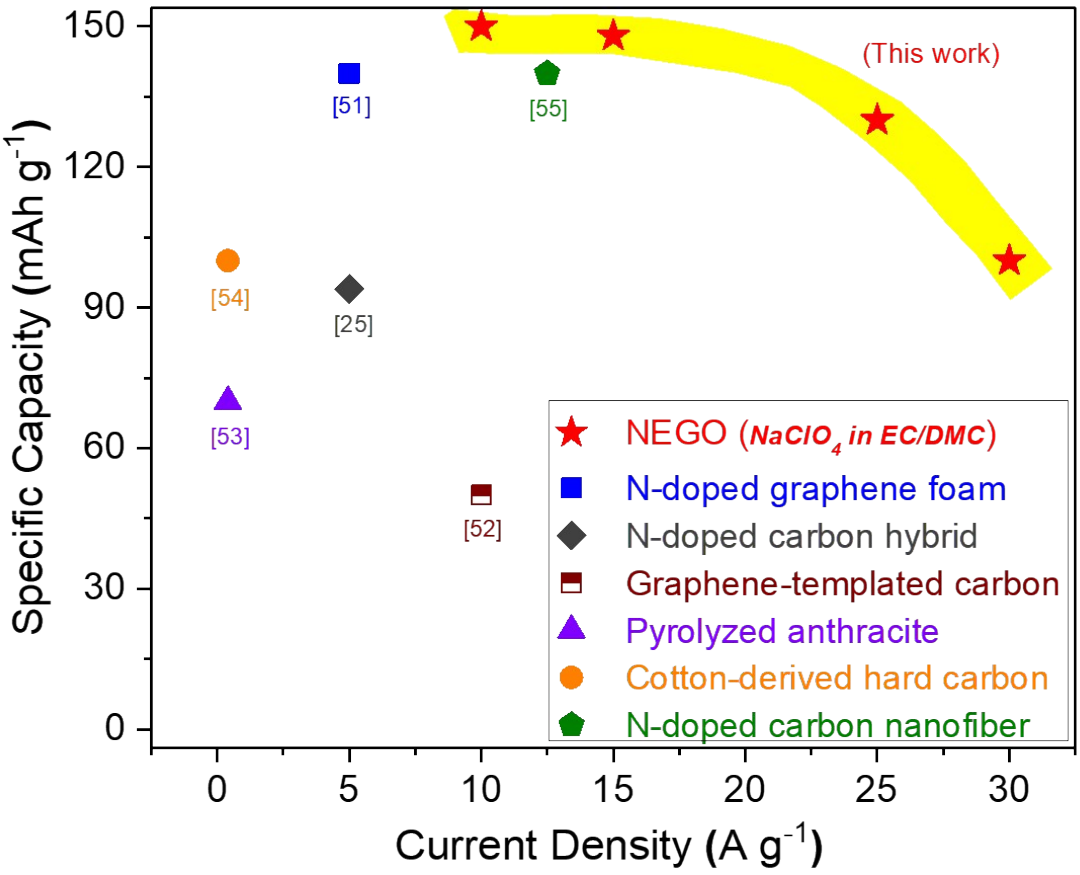

Figure S23. Comparison of rate ability between NEGO (ester-based electrolyte: EC/DMC) and other carbon-based materials in SIBs under various current densities.

Table S1. Elemental analysis of C, N and O in GO, EGO and NEGO samples.

Element content (at. %)	C	O	N
GO	65.03	34.07	0
EGO	88.81	11.19	0
NEGO	87.04	8.77	4.18

Table S2. Diffusion coefficients of NEGO before and after the formation of SEI in LIB and SIB.

	LIB-1st	**LIB-SEI**	**SIB-1st**	**SIB-SEI**
σ_w	43.9	191.9	157.3	146.5
D (*10^{-13} m^2/s)	37	1.9	2.9	3.3

Table S3. Diffusion lengths of NEGO working in ether-based electrolyte (DIGLYME) under different current densities.

Current density (A g^{-1})	0.1	0.5	1	2	5	10	20	30
L (μm)	59.7	24.8	16.5	11.4	6.8	4.5	3.8	2.2

Table S4. Capacitance contribution of NEGO in ether-based and ester-based electrolytes under various scan rates.

Scan rates (mV/s)	**1**	**2**	**10**	**20**	**50**	**200**	**300**	**400**	**500**
DIGLYME (%)	46.8	48.6	56.0	60.2	66.4	81.1	87.9	93.7	99.2
EC/DMC (%)	23.8	33.9	32.2	35.7	42.1	65.5	75.3	84.8	93.5

Table S5. Electrochemical properties of different materials for SIB anodes.

Name	Electrochemical Properties	*Reference*
Nitrogen-doped expanded graphite oxide	100 mAh g^{-1} after 5000 cycles at 10 A g^{-1}; Rate capacity: 100 mAh g^{-1} at 30 A g^{-1};	*This work*
Nitrogen-doped graphene foam	600 mAh g^{-1} after 150 cycles at 0.5 A g^{-1}; Rate capacity: 140 mAh g^{-1} at 5 A g^{-1};	[1]
Sandwich-like hierarchically porous carbon/graphene composite	200 mAh g^{-1} after 1000 cycles at 0.5 A g^{-1}; 150 mAh g^{-1} after 10000 cycles at 5 A g^{-1};	[2]
Graphene-based nitrogen-doped carbon sandwich nanosheets	93.3 mAh g^{-1} after 250 cycles at 0.2 A g^{-1}; 141 mAh g^{-1} after 1000 cycles at 0.04 A g^{-1};	[3]
Nitrogen-doped carbon/graphene hybrid	Rate capacity: 94 mAh g^{-1} at 5 A g^{-1}; 270 mAh g^{-1} after 200 cycles at 0.05 A g^{-1};	[4]
Graphene template-derived carbon	200 mAh g^{-1} after 2000 cycles at 0.2 A g^{-1}; Rate capacity: 50 mAh g^{-1} at 10 A g^{-1};	[5]

Reference

[1] J. Xu, M. Wang, N. P. Wickramaratne, M. Jaroniec, S. Dou, L. Dai, *Adv. Mater.* **2015**, *27*, 2042.

[2] Y. Yan, Y. X. Yin, Y. G. Guo, L. J. Wan, *Adv. Energy Mater.* **2014**, *4*, 1301584.

[3] D. Li, L. Zhang, H. Chen, J. Wang, L. X. Ding, S. Wang, P. J. Ashman, H. Wang, *J. Mater. Chem. A* **2016**, *4*, 8630.

[4] H. Liu, M. Jia, B. Cao, R. Chen, X. Lv, R. Tang, F. Wu, B. Xu, *J. Power Sources* **2016**, *319*, 195.

[5] X. Zhou, X. Zhu, X. Liu, Y. Xu, Y. Liu, Z. Dai, J. Bao, *J. Phys. Chem. C* **2014**, *118*, 22426.